Biomedical Optics EXPRESS

Evaluation of burn severity *in vivo* in a mouse model using spectroscopic optical coherence tomography

Yang Zhao,[1,4] Jason R. Maher,[1,4] Jina Kim,[2] Maria Angelica Selim,[3] Howard Levinson,[2,3] and Adam Wax[1,*]

[1]*Department of Biomedical Engineering, Duke University, Durham, NC 27708, USA*
[2]*Department of Surgery, Duke University Medical Center, Durham, NC 27708, USA*
[3]*Department of Pathology, Duke University Medical Center, Durham, NC 27708, USA*
[4]*These authors contributed equally to this work*
**a.wax@duke.edu*

Abstract: Clinical management of burn injuries depends upon an accurate assessment of the depth of the wound. Current diagnostic methods rely primarily on subjective visual inspection, which can produce variable results. In this study, spectroscopic optical coherence tomography was used to objectively evaluate burn injuries *in vivo* in a mouse model. Significant spectral differences were observed and correlated with the depth of the injury as determined by histopathology. The relevance of these results to clinical burn management in human tissues is discussed.

OCIS codes: (170.6510) Spectroscopy, tissue diagnostics; (110.4500) Optical coherence tomography.

References and links

1. D. S. Kauvar, S. E. Wolf, C. E. Wade, L. C. Cancio, E. M. Renz, and J. B. Holcomb, "Burns sustained in combat explosions in Operations Iraqi and Enduring Freedom (OIF/OEF explosion burns)," Burns **32**(7), 853–857 (2006).
2. E. Finkelstein, P. S. Corso, and T. R. Miller, *The incidence and economic burden of injuries in the United States* (Oxford University Press, Oxford; New York, 2006).
3. D. C. Sainsbury, "Critical evaluation of the clinimetrics of laser Doppler imaging in burn assessment," J. Wound Care **17**(5), 193–200 (2008).
4. R. J. Talbert, S. H. Holan, and J. A. Viator, "Photoacoustic discrimination of viable and thermally coagulated blood using a two-wavelength method for burn injury monitoring," Phys. Med. Biol. **52**(7), 1815–1829 (2007).
5. M. A. Afromowitz, J. B. Callis, D. M. Heimbach, L. A. DeSoto, and M. K. Norton, "Multispectral imaging of burn wounds: a new clinical instrument for evaluating burn depth," IEEE Trans. Biomed. Eng. **35**(10), 842–850 (1988).
6. K. H. Kim, M. C. Pierce, G. Maguluri, B. H. Park, S. J. Yoon, M. Lydon, R. Sheridan, and J. F. de Boer, "In vivo imaging of human burn injuries with polarization-sensitive optical coherence tomography," J. Biomed. Opt. **17**(6), 066012 (2012).
7. J. De Boer, S. Srinivas, A. Malekafzali, Z. Chen, and J. Nelson, "Imaging thermally damaged tissue by Polarization Sensitive Optical Coherence Tomography," Opt. Express **3**(6), 212–218 (1998).
8. S. Jiao, W. Yu, G. Stoica, and L. V. Wang, "Contrast mechanisms in polarization-sensitive Mueller-matrix optical coherence tomography and application in burn imaging," Appl. Opt. **42**(25), 5191–5197 (2003).
9. M. C. Pierce, R. L. Sheridan, B. Hyle Park, B. Cense, and J. F. de Boer, "Collagen denaturation can be quantified in burned human skin using polarization-sensitive optical coherence tomography," Burns : journal of the International Society for Burn Injuries **30**(6), 511–517 (2004).
10. A. Mazhar, S. Saggese, A. C. Pollins, N. L. Cardwell, L. Nanney, and D. J. Cuccia, "Noncontact imaging of burn depth and extent in a porcine model using spatial frequency domain imaging," J. Biomed. Opt. **19**(8), 086019 (2014).
11. A. Ponticorvo, D. M. Burmeister, B. Yang, B. Choi, R. J. Christy, and A. J. Durkin, "Quantitative assessment of graded burn wounds in a porcine model using spatial frequency domain imaging (SFDI) and laser speckle imaging (LSI)," Biomed. Opt. Express **5**(10), 3467–3481 (2014).
12. J. R. Maher, V. Jaedicke, M. Medina, H. Levinson, M. A. Selim, W. J. Brown, and A. Wax, "In vivo analysis of burns in a mouse model using spectroscopic optical coherence tomography," Opt. Lett. **39**(19), 5594–5597 (2014).

#243148 Received 16 Jun 2015; revised 7 Aug 2015; accepted 10 Aug 2015; published 13 Aug 2015

13. J. Kim, W. Brown, J. R. Maher, H. Levinson, and A. Wax, "Functional optical coherence tomography: principles and progress," Phys. Med. Biol. **60**(10), R211–R237 (2015).
14. A. D. Jaskille, J. W. Shupp, M. H. Jordan, and J. C. Jeng, "Critical review of burn depth assessment techniques: Part I. Historical review," J. Burn Care Res. **30**(6), 937–947 (2009).
15. F. Robles, R. N. Graf, and A. Wax, "Dual window method for processing spectroscopic optical coherence tomography signals with simultaneously high spectral and temporal resolution," Opt. Express **17**(8), 6799–6812 (2009).
16. J. Bayliss, S. Delarosa, J. Wu, J. R. Peterson, O. N. Eboda, G. L. Su, M. Hemmila, P. H. Krebsbach, P. S. Cederna, S. C. Wang, C. Xi, and B. Levi, "Adenosine triphosphate hydrolysis reduces neutrophil infiltration and necrosis in partial-thickness scald burns in mice," J. Burn Care Res. **35**(1), 54–61 (2014).
17. S. L. Jacques, "Optical properties of biological tissues: a review," Phys. Med. Biol. **58**(11), R37–R61 (2013).
18. F. E. Robles and A. Wax, "Measuring morphological features using light-scattering spectroscopy and Fourier-domain low-coherence interferometry," Opt. Lett. **35**(3), 360–362 (2010).
19. F. E. Robles, Y. Zhu, J. Lee, S. Sharma, and A. Wax, "Detection of early colorectal cancer development in the azoxymethane rat carcinogenesis model with Fourier domain low coherence interferometry," Biomed. Opt. Express **1**(2), 736–745 (2010).
20. J. Canny, "A Computational Approach to Edge Detection," IEEE Trans. Pattern Anal. Mach. Intell. **8**(6), 679–698 (1986).
21. L. S. Hansen, J. E. Coggle, J. Wells, and M. W. Charles, "The Influence of the Hair Cycle on the Thickness of Mouse Skin," Anat. Rec. **210**(4), 569–573 (1984).
22. J. Sandby-Møller, T. Poulsen, and H. C. Wulf, "Epidermal thickness at different body sites: Relationship to age, gender, pigmentation, blood content, skin type and smoking habits," Acta Derm. Venereol. **83**(6), 410–413 (2003).
23. R. Graaff, A. C. Dassel, M. H. Koelink, F. F. de Mul, J. G. Aarnoudse, and W. G. Zijistra, "Optical properties of human dermis in vitro and in vivo," Appl. Opt. **32**(4), 435–447 (1993).
24. T. E. Matthews, M. G. Giacomelli, W. J. Brown, and A. Wax, "Fourier domain multispectral multiple scattering low coherence interferometry," Appl. Opt. **52**(34), 8220–8228 (2013).
25. T. E. Matthews, M. Medina, J. R. Maher, H. Levinson, W. J. Brown, and A. Wax, "Deep tissue imaging using spectroscopic analysis of multiply scattered light," Optica **1**(2), 105–111 (2014).

1. Introduction

Although outcomes for burn patients have improved dramatically over the past few decades, burn wounds still cause significant morbidity and mortality [1] and are estimated to cost $7.5 billion per year in the United States [2]. Outcomes are dependent upon an accurate assessment of burn depth, which predicts if the wound will heal within a few weeks after injury; a false-positive assessment leads to unnecessary surgery while a false-negative one leads to longer hospital stays, contracture, and hypertrophic scar formation. A number of techniques have been proposed for noninvasive assessment of burn injuries (including laser Doppler imaging [3], photo-acoustic imaging [4], near-infrared spectroscopy [5], polarization sensitive optical coherence tomography (PS-OCT) [6–9], spatial frequency domain imaging [10, 11], and spectroscopic optical coherence tomography (SOCT) [12, 13]), but none have been widely adopted. Clinical evaluation methods still rely primarily on subjective visual inspection, which provides limited accuracy, especially for assessing intermediate, partial-thickness burns [14]. Therefore, new technologies capable of objectively characterizing burn wounds are needed to improve patient outcomes and reduce the economic burden of these injuries.

In this paper, burn wounds of varying severity were studied *in vivo* in a mouse burn model with SOCT. Spectroscopic data were extracted through the use of a short time Fourier transform (STFT) or the recently-developed dual window (DW) method [15]. A depth-dependent analysis method is also presented and used to extract parameters correlated with the severity of the injury as determined by histopathology. The results suggest that this approach could be used to objectively assess burn wounds.

2. Experimental methods and design

All data were acquired *in vivo* from female C57BL/6 mice (Jackson Laboratories, Bar Harbor, ME) at 10-12 weeks of age and weighing between 18 and 23 grams. After anesthetization, the mice were shaved and placed in a customized mold with an 8-mm-diameter opening. The

#243148 Received 16 Jun 2015; revised 7 Aug 2015; accepted 10 Aug 2015; published 13 Aug 2015

opening was exposed to 60°C water for 5, 10, 18 or 25 seconds producing injuries ranging from superficial burns to full thickness burns [16]. This procedure was approved by the Institutional Animal Care & Use Committee at Duke University.

Following burn induction, each mouse (N = 4 total; 1 per exposure time) was imaged with a commercial, spectral-domain OCT system (Spark DRC, Wasatch Photonics Inc., Durham, NC) with a center wavelength of 850 nm, bandwidth of 155 nm, imaging depth range of 2 mm, and axial and lateral resolutions in air of 2.1 μm and 8 μm, respectively. Cross-sectional OCT images were acquired from both burned and adjacent healthy sites (32 co-located images per site; 1 burned and 1 healthy site per mouse) for comparison and the tissue was marked with India ink for registration with histopathology. Histopathology showed superficial injury with epidermal necrosis for the 5 second burn, dermal injury with collagen damage to a depth of about 200 μm for the 10 second burn, deeper injury with necrotic hair follicles and damage to a depth of about 450 μm for the 18 second burn, and injury evident down to the subcutaneous adipose tissue for the 25 second burn. For the remainder of this article, these injuries will be referred to as epidermal (EB), superficial partial thickness (SPTB), deep partial thickness (DPTB), and full thickness (FTB) burns, respectively.

Depth-resolved spectroscopic data were obtained by processing the raw interferometric signal with custom software written in MATLAB (R2013a, Mathworks, Natick, MA). The raw data were processed with an STFT or the DW method and spectra that fell below a minimum intensity threshold were discarded. A spectral window of 75 cm^{-1} was used for the STFT, resulting in a spectral resolution of approximately 5 nm and a degraded axial resolution of 60 μm. The DW method calculates the product of two spectral windows of different widths to achieve high resolution in both the spatial (time) and frequency domains. In our study, a wide window of 1400 cm^{-1} was applied resulting in an axial resolution of 3 μm in air while a narrow window of 75 cm^{-1} provided a spectral resolution of 5 nm. These parameters were chosen to match those used in a previous study [12].

The depth-resolved spectroscopic data were used to classify the tissue as burned or healthy using parameters derived from either a power-law or logistic regression classification model. In the power-law model, the spectrum associated with each pixel was fit with the expression $A\lambda^{-b}$ where λ is the wavelength and A, b are fitted parameters. The logistic regression classification model utilized principal component analysis to reduce the dimensionality of the data followed by logistic regression to form a binary predictor for each pixel as described previously [12].

3. Results

Representative data acquired from the SPTB are presented in Fig. 1. This figure shows both conventional, intensity-based OCT images obtained *in vivo* (a-b) as well as the corresponding histopathology (c-d). The conventional OCT images appear similar, making classification based on intensity alone difficult. The histopathology, however, shows clear differences between the burned [Fig. 1(d)] and healthy tissue [Fig. 1(c)] including darkly-stained cell nuclei in the burned sample that are indicative of necrosis associated with inflammation and an altered distribution of adipose cells.

Figure 2 shows the average spectra acquired from the DPTB, SPTB, and adjacent healthy tissues after processing with an STFT. The average power-law exponent across the DPTB decreased from $b = 6.7 \pm 2.9$ (mean ± standard deviation) at the healthy site to $b = 2.0 \pm 2.5$ (burned site) while the power-law exponent for the SPTB decreased from $b = 6.0 \pm 2.8$ (healthy) to $b = 4.4 \pm 3.1$ (burned). Also notice that the burned tissue spectrum shows several oscillatory features that appear similar to the absorption spectrum of adipose tissue [17]. The histopathology in Fig. 1(d) supports this observation showing that the fat cells are no longer confined beneath the dermis. Receiver operating characteristic (ROC) curves generated using the power-law or logistic regression classification model trained on data from the SPTB

#243148 Received 16 Jun 2015; revised 7 Aug 2015; accepted 10 Aug 2015; published 13 Aug 2015

sample are displayed in Fig. 2(c). The overall accuracies of 65% (power-law) and 76% (logistic regression) suggest that this approach, although previously shown to be capable of providing an accuracy of 90% in classifying severe, full-thickness burns [12], may not be sufficient for elucidating the more subtle differences in less severe, partial-thickness burns.

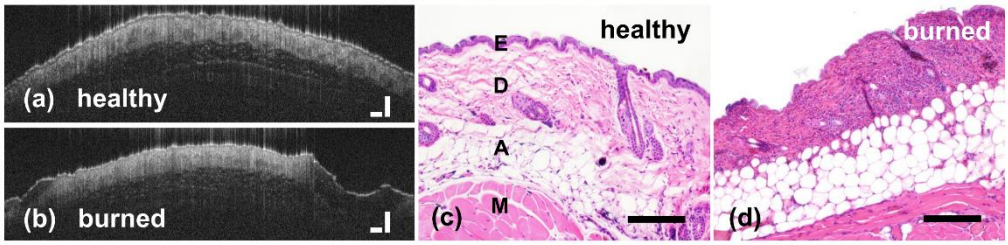

Fig. 1. OCT images of (a) healthy and (b) burned (SPTB) mouse tissue *in vivo*. Corresponding histopathology is shown in (c) and (d). (c) Healthy tissue layers include the E-epidermis, D-dermis, A-adipose, and M-muscle. (d) Burned tissue shows darkly-stained cell nuclei indicative of inflammation in the superficial layer. (Scale bars 250 μm.)

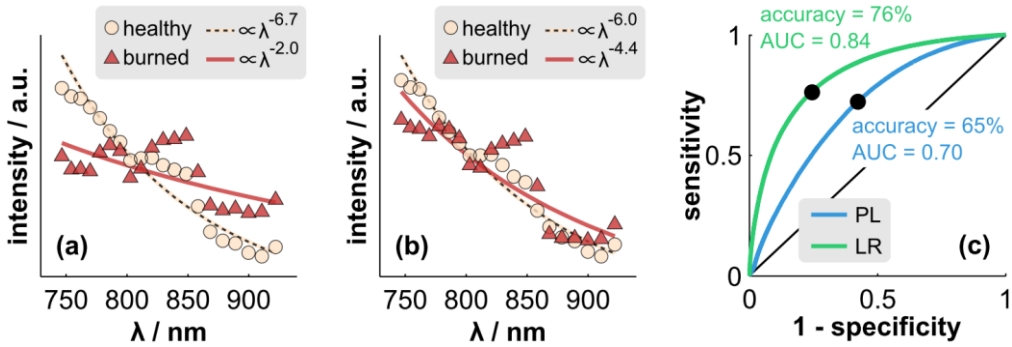

Fig. 2. Average spectra acquired from the DPTB (a) and SPTB (b) samples and adjacent healthy tissue. Spectra were downsampled for display purposes and error bars were omitted because the 95% confidence intervals are smaller than the markers. (c) ROC curves generated with the power-law (PL) and logistic regression (LR) classification models. The area under the curve (AUC) and accuracy (calculated at the location of the black dot) of each method are also listed.

Similar analyses were performed using the DW method to extract spectroscopic data. However, as in a previous study [12], the STFT produced superior classification accuracy in burn discrimination. It should be noted that although the DW method is capable of measuring bulk tissue properties, it was developed for high resolution imaging of single cellular particles [18, 19] and may not be ideally-suited to measure macroscopic changes associated with burn wounds. The remainder of this article will focus on spectroscopic data extracted with STFTs.

In the above analysis, spectroscopic data from all depths were used to train the power-law and logistic regression classification models. In order to improve diagnostic accuracy and provide an estimate of burn depth, we developed a depth-dependent analysis method. A customized Canny edge detector [20] was used to determine the location of the tissue surface and nine, 25-μm-thick layers were segmented from the surface down to a depth of 225 μm. The thickness of the segmented layers was chosen to satisfy the Nyquist-Shannon sampling theorem given the spatial resolution of 60 μm provided by the STFT. Finally, separate power-law and logistic regression classification models were trained for each burn severity and each layer below the tissue surface. These classification models were not used to predict the severity or depth of injury, but rather to classify each pixel within an image as either healthy or burned.

#243148 Received 16 Jun 2015; revised 7 Aug 2015; accepted 10 Aug 2015; published 13 Aug 2015

Figure 3(a) shows the percentage of pixels in each layer classified as burned by the depth-dependent logistic regression models. As expected, the percentage increases with burn severity and decreases with depth (because the most severe damage is generally observed in the superficial layers). Figure 3(b) presents the ROC curve associated with classification of the pixels in the surface layers (0-25 μm depth) of the SPTB and adjacent healthy tissue. This model achieved an overall accuracy of 90%. For comparison, the original logistic regression model, which used spectroscopic data from all depths for classification, achieved an accuracy of 76% [Fig. 2(c)]. We observed a similar improvement with each depth-dependent classification model at the tissue surface (0-25 μm depth) as the classification accuracies increased from 91% to 98%, 86% to 90%, and 52% to 59% for the FTB, DPTB, and EB, respectively. It should be noted that it is not possible to generate ROC curves associated with deeper layers because the health of the tissue is not known on a pixel-by-pixel basis at these depths. We therefore chose to report classification accuracy at the surface of the tissue. The spectroscopic differences between burned and healthy tissue can also be visualized by color-coding the OCT images. Figure 4 displays false-color images of the SPTB and adjacent healthy tissue generated using logistic regression with [Fig. 4(b)] and without [Fig. 4(a)] the depth-dependent analysis method. The figure shows that the colors derived from the depth-dependent analysis method are more uniform than those derived from the original classification model.

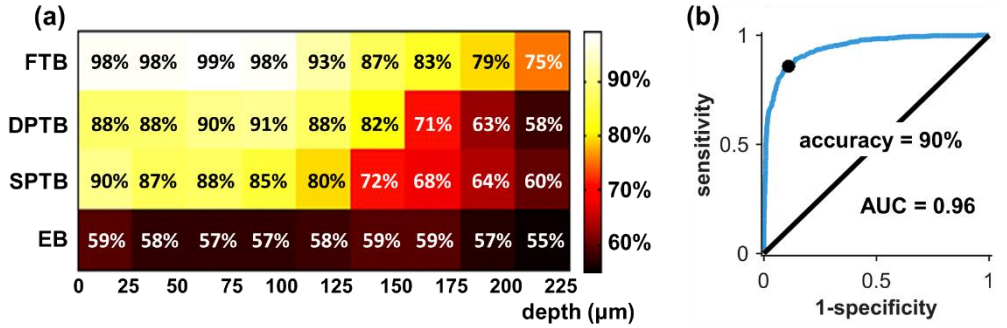

Fig. 3. (a) Percentage of pixels classified as burned using depth-dependent logistic regression. (b) ROC curve associated with this model applied to the data from the surface layers (0-25 μm) of the SPTB [for comparison to Fig. 2(c)] and adjacent healthy tissue. The area under the curve (AUC) and accuracy (calculated at the location of the black dot) are also listed.

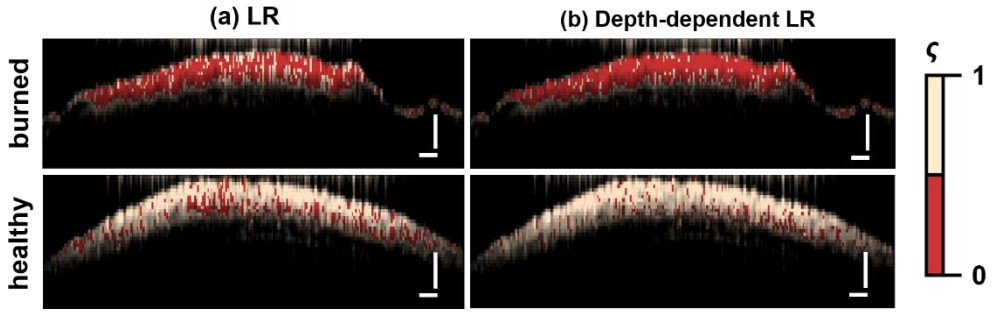

Fig. 4. Color coded OCT images based on (a) original logistic regression (LR) model and (b) depth-dependent LR model. (Scale bars 250μm.)

The depth-dependent analysis method was also used to determine the fitted power-law exponent as a function of depth for each sample. A normalized exponent b_{rel} was calculated as $b_{rel}(z) = b_{burned}(z) / b_{healthy}(z)$, where $b_{burned}(z)$ is the average power-law exponent associated with the burned tissue at depth z and $b_{healthy}(z)$ is the average exponent of the

#243148 Received 16 Jun 2015; revised 7 Aug 2015; accepted 10 Aug 2015; published 13 Aug 2015

adjacent healthy tissue at the same depth. As shown in Fig. 5(a), the more severe injuries typically yielded lower normalized values for the exponents. The figure also shows that b_{rel} generally increased with depth in the tissue, indicating that the severity of the burn decreased with depth. The only exception to this trend is the data associated with the EB, where b_{rel} remained relatively stable across all depths, suggesting that epidermal burns do not significantly alter tissue scattering or absorption in the near infrared spectral range.

Although our system has a maximum imaging range of 2 mm, the practical penetration depth in murine skin is limited by scattering to a few hundred microns and we were therefore unable to image through the entire DPTB and FTB. Despite the limited penetration depth, we did observe correlations between the injury depths, which ranged between 0 and approximately 500 μm, and the power-law exponents extracted from the superficial layers of the tissue. For the range of imaging depths examined here (0-225 μm), the correlations were all statistically significant and ranged from –0.93 at the surface layers (0-25 μm depth) to –0.9998 with the best correlation observed by using spectral information from a depth of 175 μm below the tissue surface for discrimination [r = –0.9998, p<0.001, Fig. 5(b)].

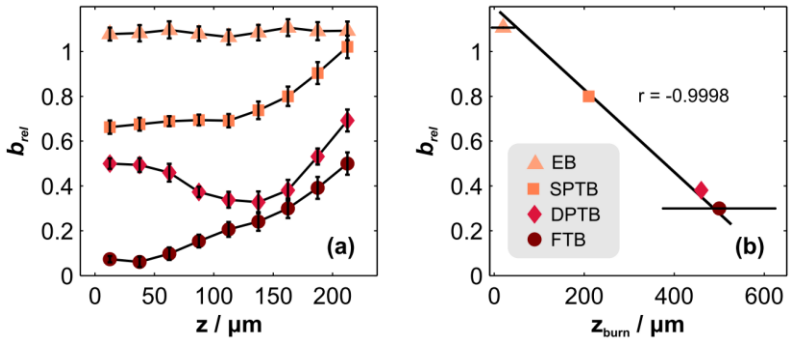

Fig. 5. (a) Normalized power-law exponents of all four burn severities versus imaging depth. Error bars represent the standard deviation of the exponent. (b) Correlation between the average normalized power-law exponents measured at a depth of 175 μm and the depth of the injury (z_{burn}) determined by histopathology. Error bars represent the estimated range of injury determined by the histopathologist. Note that the collagen structure in the FTB sample collapsed causing the tissue to flatten and resulting in a large uncertainty in the measured burn depth.

4. Discussion and conclusions

In this study, SOCT was used to analyze and classify burn injuries of varying severities *in vivo* in a mouse model. A depth-dependent analysis method was presented that enhanced classification accuracy and the spectroscopic data were correlated with burn depth as determined by histopathology. A strong negative correlation (r = –0.9998) was observed between the depth of the injury and a normalized power-law exponent suggesting that this approach could be used to assess burn depth.

The main drawback of using near-infrared SOCT for burn injury assessment is the limited penetration depth, which is a few hundred microns in skin. Although this is sufficient to image a large portion of dermal mouse tissue [21], the penetration depth may preclude the use of SOCT in assessing the thicker epidermal and dermal layers found in human skin [22, 23]. Clinically, the classification and management of burns depends upon the extent of the injury in both of these layers. Although our results suggest that spectral analysis of superficial tissue could be used as a surrogate measure of the health of deeper dermal layers, new spectroscopic techniques with improved penetration depth [24, 25] could potentially be used in conjunction with the analysis methods presented here to directly assess burn depth in human patients.

#243148 Received 16 Jun 2015; revised 7 Aug 2015; accepted 10 Aug 2015; published 13 Aug 2015

Acknowledgments

This work was supported by the NIH (R01 HD072702), a subcontract from the Medical College of Wisconsin for R01 CA158319 (L. Kresty, PI), and a research training grant from LifeCell. The authors also wish to acknowledge Volker Jaedicke for assistance acquiring the SOCT data and Manuel Medina for assistance preparing the histopathology slides.

#243148 Received 16 Jun 2015; revised 7 Aug 2015; accepted 10 Aug 2015; published 13 Aug 2015